

**Compensation for the Eddy Current Effect
in the APS Storage Ring Vacuum Chamber**

Y. Chung

Abstract

The amplitude attenuation and the phase shift of the correction magnet field inside the APS storage ring vacuum chamber due to the eddy current effect were measured. A circuit to compensate for this effect was then inserted between the signal source and the magnet power supply. The amplitude was restored with an error of less than 20 % of the source signal amplitude and the phase shift was reduced from 80° to 12° at 10 Hz.

1. Introduction

A number of correction dipole magnets will be installed around the APS storage ring to stabilize the beam against the low frequency vibration below 25 Hz from various sources. The correction magnet system consists of 240 vertical field dipole magnets for horizontal corrections and 78 vertical/horizontal field magnets for horizontal and vertical corrections. A detailed description of the design specification parameters for these magnets can be found in Ref. 1.

The displacement of the quadrupole magnets due to vibration has the most significant effect on the stability of the positron closed orbit in the storage ring. A small displacement of the quadrupole magnet leads to a large distortion of the closed orbit, and hence, the growth of the emittance. The internal source of vibration includes the mechanical motion of the various components of the ring, such as rotating machinery, pumps, compressors and high vacuum equipment. This internal vibration can be reduced by balancing the equipment and isolating the sources. The primary external source of the low frequency vibration is the ground motion of approximately 20 μm amplitude, with frequency components concentrated below 10 Hz. These low frequency vibrations can be corrected using the correction magnets, whose field strengths are controlled individually through the feedback loop comprising the beam position monitoring (BPM) system.

The AC component of the correction magnet field, externally applied to the vacuum chamber, induces eddy current inside the aluminum vacuum chamber. Since this eddy current is proportional to the amplitude and the frequency of the AC field, it is concentrated immediately below the outer surface of the conducting vacuum chamber. This current, which flows in the direction cancelling the original field due to the magnet current, decreases not only the field inside the vacuum chamber but also the field outside in the vicinity of the vacuum chamber. How far the field strength decreases in the

presence of the vacuum chamber relative to the otherwise unperturbed field depends on the geometry of the magnet as well as the vacuum chamber and is beyond the scope of the present article.

With the conductivity $\sigma = 3.54 \times 10^7 / \Omega \cdot \text{m}$ for the aluminum used in the fabrication of the APS storage ring, the wavenumber k inside the aluminum is given by²

$$\begin{aligned} k &\simeq (1 + i) \sqrt{\frac{\mu\omega\sigma}{2}} \\ &= 0.12 (1 + i) \sqrt{f(\text{Hz})} (\text{cm}^{-1}) \end{aligned} \quad (1)$$

assuming the harmonic time dependence $e^{-i\omega t}$ and the spatial dependence of $e^{ik \cdot x}$ for a simple slab geometry. Then, for the aluminum of thickness 12.7 mm, the attenuation factor a and the phase shift $\Delta\phi$ can be written as

$$\begin{aligned} a &= \exp(-0.152\sqrt{f}), \\ \Delta\phi &= 0.152\sqrt{f} = 8.73^\circ \times \sqrt{f}. \end{aligned} \quad (2)$$

However, as mentioned in the preceding paragraph, Eq. (2) alone cannot be relied upon for the estimation of the field attenuation and the phase shift in the vacuum chamber relative to the unperturbed field. Given the partial cancellation of the field outside the vacuum chamber due to the eddy current under the surface, Eq. (2) is an underestimation of the actual attenuation and phase shift. This is confirmed by the result³ obtained using the computer code PE2D with the actual geometry of the correction magnet and the vacuum chamber, which shows much larger amplitude attenuation and phase shift than predicted by Eq. (2). At this time, no correction magnet to be used in the APS storage ring has been built. Our goal now is, therefore, to design a compensation circuit and to test the feasibility of compensating for the undesired attenuation and phase shift simultaneously below 20 Hz. This warrants the accurate measurement of these quantities using the vacuum chamber and the magnet of geometry as close as possible to the actual ones.

In this article, the measurement results of the field attenuation and the phase shift of the correction magnet field in the APS storage ring vacuum chamber are presented. In Section 2, the measurement setup is described, and the results are presented in Section 3. Section 4 describes the measurement using a circuit designed to compensate for the eddy current and the low-pass filtering by the magnet, which was inserted between the signal source and the magnet power supply. In Section 5, the summary of this work and a suggestion for possible future work are given.

2. Setup of the Measurement

The source signal was provided by a function generator (model 166) manufactured by Wavetek. For the measurement of the amplitude attenuation and the phase shift, sine waves of frequency between 1 and 25 Hz were used. The data was taken at 1, 2, 4, ..., 20, 22, and 25 Hz. Square waves and triangular waves were also used to measure the rise time of the magnetic field inside the vacuum chamber or to demonstrate the performance of the compensation circuit inserted between the function generator and the power supply.

To measure the amplitude attenuation and the phase shift of the AC magnetic field inside the APS storage ring vacuum chamber relative to the unperturbed field, a setup for measurement as shown in Fig. 1 was made. The specification of the magnet, which was used in the electron cooling ring experiment at FNAL,⁴ is given in Table 1. With the inductance $L = 10$ mH and the coil resistance $R_c = 25$ m Ω , the time constant of the magnet τ_c is equal to $L/R_c = 400$ ms. In order to reduce the time constant, a water-cooled stainless steel resistor of $R = 0.2$ Ω was connected in series to the magnet. This reduced the time constant τ to 44 ms.

The current flowing through the magnet was monitored by a scope which displays the signal from the current-voltage transducer. The transducer and the scope are symbolically drawn as a combination of a small resistor and a scope (V_c) as shown in Fig. 1.

For the magnetic field measurement, a Hall probe (model FP039/U) and a gaussmeter (model 912) manufactured by Dowty RFL Industries were used. The gaussmeter gives a digital reading of the magnetic field strength in Gauss and also provides a scope output. The signal from the scope output is 5 kHz sine wave amplitude modulated by the Hall probe signal, which is displayed on the scope marked as V_g in Fig. 1.

When two signals were compared, e. g., when the current measured by V_c and the magnetic field strength measured by V_g were compared to calculate the field attenuation and the phase shift due to the vacuum chamber, these signals were displayed synchronously on a single scope equipped with multiple channels sharing the same trigger signal.

3. Measurements and Results

The linearity of the Hall probe response to the applied magnetic field was checked by measuring the current (V_c from the current-voltage transducer) and the magnetic field strength (V_g from the gaussmeter scope output) without the vacuum chamber. The digital reading (G) of the field on the gaussmeter was also recorded for each measurement. This was done for both DC and AC signals. For the case of the DC linearity, the ratios V_c/G and V_g/G were measured as functions of the field strength G to check if they stay constant. From this measurement, we also obtained the calibration factors for the transducer signal V_c and the gaussmeter signal V_g . For the case of the

AC linearity, the ratio V_g/V_c was measured and it was checked if it stays constant for different frequencies. As shown in Fig. 2 (a) for the ratios V_c/G and V_g/G as functions of the DC field strength G , the response of the Hall probe and the digital reading on the gaussmeter is highly linear to the applied DC signal. The result of a similar procedure for the AC linearity check is shown in Fig. 2 (b). The DC bias level was set at 1,200 G and the power supply was modulated at various frequencies. The AC field amplitude was set at 25 % of the DC bias level, i. e., 300 G. No attenuation or phase shift in the Hall probe response was observed as a function of the driving current in the magnet. In Fig. 2 (b), the horizontal axis is the modulation frequency in Hz and the vertical axis is the ratio V_g/V_c after normalization using the proportionality constants obtained in the DC linearity check (see Fig. 2 (a)). The voltage reading on the scope was converted to field strength in Gauss before taking the ratio. The result clearly shows that there is no appreciable deviation from linearity in the response of the Hall probe to the AC field within the frequency range of our interest.

After the linearity check on the Hall probe response to DC and AC signals was completed, the storage ring vacuum chamber was inserted in the magnet bore and placed at the vertical center as shown in Fig. 1 (a). The Hall probe was then placed at the center of the positron beam chamber. Since the entire cross section of the vacuum chamber was larger than could fit into the magnet bore, the antechamber was cut away, leaving only the positron beam chamber and the photon beam channel. This will have negligible effect on the measurement due to the large ratio of horizontal to vertical dimensions of the photon beam duct. In other words, the magnetic field in the positron beam chamber will be affected very little by the 'leakage' of the field from far out.

Since the circuit comprising the magnet and the resistors are basically a low-pass filter, a signal with high frequency will be attenuated and delayed by up to 90° phase

shift. These amplitude attenuation and phase shift are added onto those due to the presence of the vacuum chamber and should be measured separately. Let a_v and a_m be the attenuation factors due to the vacuum chamber and the magnet, respectively, and let $\Delta\phi_v$ and $\Delta\phi_m$ be the phase shifts. Then the overall attenuation factor a_t and the overall phase shift $\Delta\phi_t$ will be

$$\begin{aligned} a_t &= a_v a_m, \\ \Delta\phi_t &= \Delta\phi_v + \Delta\phi_m. \end{aligned} \tag{3}$$

The measurement consists of comparing the amplitudes and the relative horizontal positions of the peaks of the two sine waves displayed on the scope. One is the reference signal and the other is the measurement signal. Two such measurements were made to determine a_v , $\Delta\phi_v$ and a_m , $\Delta\phi_m$. To measure a_v and $\Delta\phi_v$, the current in the magnet, which was converted to voltage V_c by the transducer, was used for reference and the Hall probe signal V_g was compared with V_c . Similarly, to measure a_m and $\Delta\phi_m$, the driving signal V_f from the function generator was used for reference and the signal V_c was compared against V_g . Figure 3 shows the results of these measurements, (a) for the attenuation factors and (b) for the phase shifts. They are also tabulated in Table 2 along with the corrections obtained using the compensation circuit described in the next section. It is to be noted that while the phase shift due to the magnet is always smaller than 90° , the phase shift due to the vacuum chamber can increase without limit, as can be seen in Eq. (2). The comparison between measurement results and Eq. (2), however, shows significant difference between them. The actual field inside the vacuum chamber decreases more rapidly with frequency and lags further behind the magnet current than was estimated without considering the modification of the field outside the vacuum chamber.

4. Compensation Circuit

In order to restore the magnetic field inside the vacuum chamber to the same shape as the driving signal, it is necessary to amplify the attenuated frequency components and to advance their phases accordingly. Consider the following relation.

$$\begin{aligned} V_c(t) &= \int d\omega \tilde{V}_c(\omega) e^{-i\omega t}, \\ V_g(t) &= \int d\omega a(\omega) e^{i\Delta\phi(\omega)} \tilde{V}_c(\omega) e^{-i\omega t}. \end{aligned} \quad (4)$$

Here, $V_c(t)$ is the unperturbed field and $V_g(t)$ is the field inside the vacuum chamber, and $\tilde{V}_c(\omega)$ and $\tilde{V}_g(\omega)$ are the Fourier transforms. If $\Delta\phi(\omega)$ is close to 90° and if $a(\omega)$ behaves like ω^{-1} within the frequency range where $|\tilde{V}_c(\omega)|$ is appreciably large, then $V_g(t)$ is simply the time integration of $V_c(t)$ except for a real multiplication factor. In this case, the compensation can be achieved by feeding the differentiation of the driving signal to the magnet.

Let $V_f(t)$ be the source signal and let $\tilde{V}_f(\omega)$ be its Fourier transform. The ideal compensation circuit would then modify the source signal such that

$$\tilde{V}_c(\omega) = \frac{1}{a(\omega)} e^{-i\Delta\phi(\omega)} \tilde{V}_f(\omega). \quad (5)$$

This can be partially achieved by using a simple circuit element shown in Fig. 4 (a). In the low frequency limit, the output signal V' will be in phase with the input signal V , but the ratio V'/V will be the same as $R_2/(R_1 + R_2)$. As the frequency of the input signal increases, the total impedance Z of the combination of R_1 and C will become more and more capacitive and its absolute value will decrease. Therefore, the output signal will precede the input signal in phase and the amplitude will increase with frequency. In the high frequency limit, Z approaches zero, and V' will be the same as V with no phase difference. The maximum phase advance achievable with this

circuit depends on the ratio R_1/R_2 and will occur at some frequency ω satisfying

$$R_1 < \frac{1}{\omega C} < R_2.$$

Assuming harmonic time dependence $e^{-i\omega t}$ and putting $r = R_1/R_2$ and $\tau = R_1 C$, the exact relation between V and V' is

$$\frac{V'}{V} = a'(\omega)e^{-i\Delta\phi'(\omega)}, \quad (6)$$

where

$$a'(\omega) = \frac{[\{1 + r + (\omega\tau)^2\}^2 + (r\omega\tau)^2]^{\frac{1}{2}}}{(1+r)^2 + (\omega\tau)^2}, \quad (7)$$

$$\Delta\phi'(\omega) = \tan^{-1}\left(\frac{r\omega\tau}{1+r+(\omega\tau)^2}\right).$$

This circuit has two disadvantages. One is that the low frequency components are attenuated significantly due to large r . Secondly, it does not have the isolation property needed to shift the phase by more than 90° . These problems can be solved easily by adding an op-amp at the output terminal as shown in Fig. 4 (b). The op-amps A1 and A2 amplify the signal by up to 100 and 10 times, respectively, and isolate the two stages from other circuit elements. A3 is an inverting adder for DC biasing and A4 re-inverts the signal. The first stage compensates for the eddy current effect in the vacuum chamber and the second stage compensates for the low-pass filtering by the magnet. The parameters r and τ were chosen such that the low frequency behavior of $\Delta\phi'$ follows the measured values as closely as possible up to 10 Hz while maintaining $aa' \sim 1$. If we let a'_v , $\Delta\phi'_v$, a'_m and $\Delta\phi'_m$ be the amplification and the phase correction by the first and the second stages, then the overall compensation will be represented by

$$a'_t = a'_v a'_m, \quad (8)$$

$$\Delta\phi'_t = \Delta\phi'_v + \Delta\phi'_m.$$

Table 2 summarizes the preceding analysis of the compensation circuit and the measurement results. It lists the measured values (unprimed) for the attenuation and the phase shift and the calculated values (primed) for the amplification and the phase shift due to the two compensation stages shown in Fig. 4 (b). There are some deviations in aa' and $\Delta\phi - \Delta\phi'$ from the ideal values, i. e., 1 for aa' and 0 for $\Delta\phi - \Delta\phi'$. In the case of the magnet, the deviations are negligibly small and may be further corrected by adjusting the parameters r_m and τ_m . In the case of the vacuum chamber, though, the deviations are relatively large. This rather large difference is due to the fact that, unlike the magnet, the vacuum chamber can shift the phase without any limit, while a single compensation stage can correct the phase by only up to 90° . However, unless the source signal, e. g., the vibrational motion that needs to be corrected, has broad-band spectrum reaching beyond 10 Hz, these deviations will not pose a problem.

With the compensation circuit inserted between the signal source and the power supply, $\tilde{V}_g(\omega)$ can be written in terms of $\tilde{V}_f(\omega)$ as

$$\tilde{V}_g(\omega) = a_t(\omega)a'_t(\omega) e^{i(\Delta\phi_t(\omega) - \Delta\phi'_t(\omega))} \tilde{V}_f(\omega). \quad (9)$$

$a_t(\omega)$, $a'_t(\omega)$, $\Delta\phi_t(\omega)$ and $\Delta\phi'_t(\omega)$ are given by Eqs. (3) and (8). Direct measurements on $a_t(\omega)a'_t(\omega)$ and $\Delta\phi_t(\omega) - \Delta\phi'_t(\omega)$ were made and the results are shown in Fig. 5 together with the calculated predictions, which show good agreement between them.

As a demonstration to show how well the compensation circuit works, triangular waves of $f_0 = 2$ and 3 Hz were used as the source signal and compared with the magnetic field inside the vacuum chamber. Since a triangular wave contains the odd harmonics ($m = 1, 3, 5, \dots$) of the fundamental frequency f_0 , with the amplitudes proportional to $1/m^2$, the dominant components in the 2 Hz triangular wave are 2, 6, and 10 Hz. On the other hand, for the 3 Hz wave, 3, 9, and 15 Hz are dominant. The comparisons are shown in Figs. 6 and 7. While the 2 Hz wave is restored almost perfectly, the

3 Hz wave is not, because of the higher frequency components which are inadequately compensated for by the circuit.

5. Summary

In the preceding sections, the measurements performed on the field attenuation and the phase shift due to the APS storage ring vacuum chamber and the correction magnet were described. Because of the thickness of the APS storage ring vacuum chamber, the eddy current induced by the time-varying field of the correction magnet causes significant delay in the penetration of the magnetic field into the storage ring. The finite inductance of the magnet adds to this effect. As a solution to correct this problem, a simple circuit was designed and inserted between the signal source and the magnet power supply. The compensation was almost complete below 10 Hz, and between 10 and 20 Hz, more than 85 % of the phase shift was corrected. The amplitude attenuation tends to be slightly overcompensated by approximately 15 %. If the vibration source has negligibly small components beyond 10 Hz as expected, this deviation from the ideal compensation will not pose a problem.

The present work considered only the open-loop compensation without any feedback from the resultant magnetic field inside the vacuum chamber. In case a stationary positron beam is desired at the correction magnet location for a wider range of frequency, a closed-loop feedback compensation may be considered. In this scheme, the magnetic field strength is derived using photon/positron beam position monitors and is then compared with the source signal. The difference of these two signals is then amplified and fed into the power supply, which then corrects the magnet field strength. Since this procedure is almost instantaneous compared to the vibration to be corrected,

near perfect compensation is possible for a much wider range of frequency than can be done with the open-loop compensation. Detailed analysis and measurements similar to those presented in this article will be performed and published separately in the near future.

Acknowledgements

The author would like to thank J. Bridges for suggesting the compensation technique and R. Biwer for his efforts in bringing the magnet from Fermilab. L. Teng, E. Crosbie and L. Turner are to be thanked for the stimulating discussions on this work, and G. Sprau, T. Smith, and D. Voss are also to be thanked for their technical assistance in the measurement.

References

¹APS Design Handbook, ANL (1989).

²J. Jackson, Classical Electrodynamics, (John Wiley & Sons, 1975), p.297.

³L. Turner, private communication.

⁴Fermilab Electron Cooling Experiment, Design Report, FNAL (1978).

Tables

Field strength	4.3 kG
Magnet length	48 in.
Magnet gap	3.25 in.
Coil aperture	12 in.
Field aperture	± 4.00
Field quality ($\Delta B/B$ within 3 in.)	$\pm 10^{-4}$
Coil turns (top and bottom)	40
Copper conductor cross section	0.46 in. \times 0.46 in.
Water cooling hole diameter	0.25 in.
Conductor corner radius	0.063 in.
Conductor current	711 A
Magnet inductance	0.010 H
Coil resistance	0.025 Ω
Voltage drop	17.8 V
Power	12.6 kW
Cooling water pressure	65 psi
Number of water paths	4
Water flow	4.4 gpm
Temperature rise	13.1°C
Outside dimensions	10 in. \times 22 in.
Iron weight (approx.)	2,100 lb
Copper weight	288 lb

Table 1: Specifications of the magnet used in this measurement.

f (Hz)	a_v	a'_v	$a_v a'_v$	a_m	a'_m	$a_m a'_m$
0.0	1.00	1.00	1.00	1.00	1.00	1.00
1.0	0.96	1.04	0.99	0.98	1.00	0.99
2.0	0.89	1.14	1.02	0.96	1.01	0.97
4.0	0.74	1.49	1.10	0.94	1.03	0.96
6.0	0.59	1.94	1.14	0.91	1.07	0.97
8.0	0.48	2.43	1.16	0.87	1.12	0.97
10.0	0.38	2.94	1.13	0.85	1.18	1.00
12.0	0.34	3.46	1.19	0.80	1.25	1.00
14.0	0.30	3.99	1.19	0.77	1.33	1.02
16.0	0.25	4.53	1.15	0.71	1.41	1.01
18.0	0.22	5.07	1.10	0.68	1.50	1.02
20.0	0.20	5.61	1.11	0.65	1.60	1.03
22.0	0.18	6.15	1.11	0.64	1.69	1.08
25.0	0.15	6.97	1.02	0.61	1.84	1.12

f (Hz)	$\Delta\phi_v$	$\Delta\phi'_v$	$\Delta\phi_v - \Delta\phi'_v$	$\Delta\phi_m$	$\Delta\phi'_m$	$\Delta\phi_m - \Delta\phi'_m$
0.0	0	0	0	0	0	0
1.0	14	15	-1	3	3	0
2.0	26	29	-3	9	7	2
4.0	48	47	1	13	13	0
6.0	61	58	3	21	19	2
8.0	72	64	8	27	24	3
10.0	81	69	12	31	29	2
12.0	86	71	15	36	33	3
14.0	90	73	17	40	37	3
16.0	96	75	21	42	40	2
18.0	101	76	25	43	43	0
20.0	104	77	27	46	45	1
22.0	106	77	29	48	47	1
25.0	112	78	34	54	49	5

Table 2: Compensation for the attenuation and the phase shift due to the vacuum chamber and the magnet. The phase shifts are expressed in degrees. The parameters r and τ were: $r_v = 100$, $r_m = 10$, $\tau_v = 0.044$, $\tau_m = 0.01$.

Figure Caption

- Fig. 1 Measurement setup for the attenuation and the phase shift of the magnetic field inside the APS storage ring vacuum chamber: (a) a section of the vacuum chamber cut short to fit into the magnet bore, (b) the electrical connection.
- Fig. 2 The result of the DC and AC linearity check on the Hall probes. (a) The ratios V_c/G and V_g/G as function of field strength G for DC linearity check. V_c and V_g are the signal from the transducer and the Gaussmeter, respectively. G is the digital reading of the magnetic field strength from the Gaussmeter. (b) The ratio V_c/V_g after normalization using the calibration factors obtained in (a).
- Fig. 3 The result of the measurement on (a) the attenuation and (b) the phase shift as functions of frequency f due to the storage ring vacuum chamber and the magnet. The attenuation factors a_v and a_m were normalized to 1 at $f = 0$.
- Fig. 4 (a) A single compensation stage without amplification. (b) The compensation circuit used to correct the attenuation and the phase shift by the vacuum chamber and the magnet. The first stage (A1) compensates for the Eddy current effect in the vacuum chamber and the second stage (A2) compensates for the low-pass filtering by the magnet.
- Fig. 5 The plotting of (a) $a_t a'_t$ and (b) $\Delta\phi_t - \Delta\phi'_t$. The measured values are indicated by the solid circles and the calculated predictions (see Table 2) are indicated by the solid curve.

Fig. 6 The restoration of the triangular wave of 2 Hz using the compensation circuit. The upper solid white lines are the source signals and the envelopes of the lower AM signals represent the magnetic field inside the vacuum chamber. The comparisons are shown (a) without the compensation circuit and (b) with the compensation circuit.

Fig. 7 The restoration of the triangular wave of 3 Hz using the compensation circuit. The upper solid white lines are the source signals and the envelopes of the lower AM signals represent the magnetic field inside the vacuum chamber. The comparisons are shown (a) without the compensation circuit and (b) with the compensation circuit.

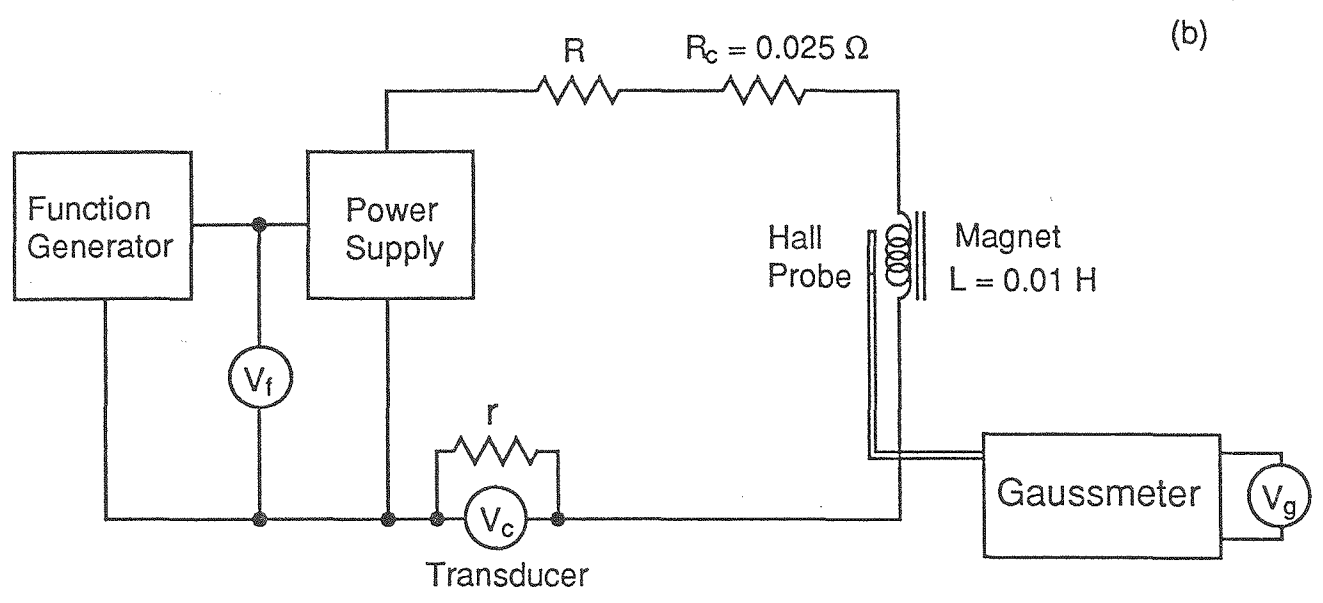
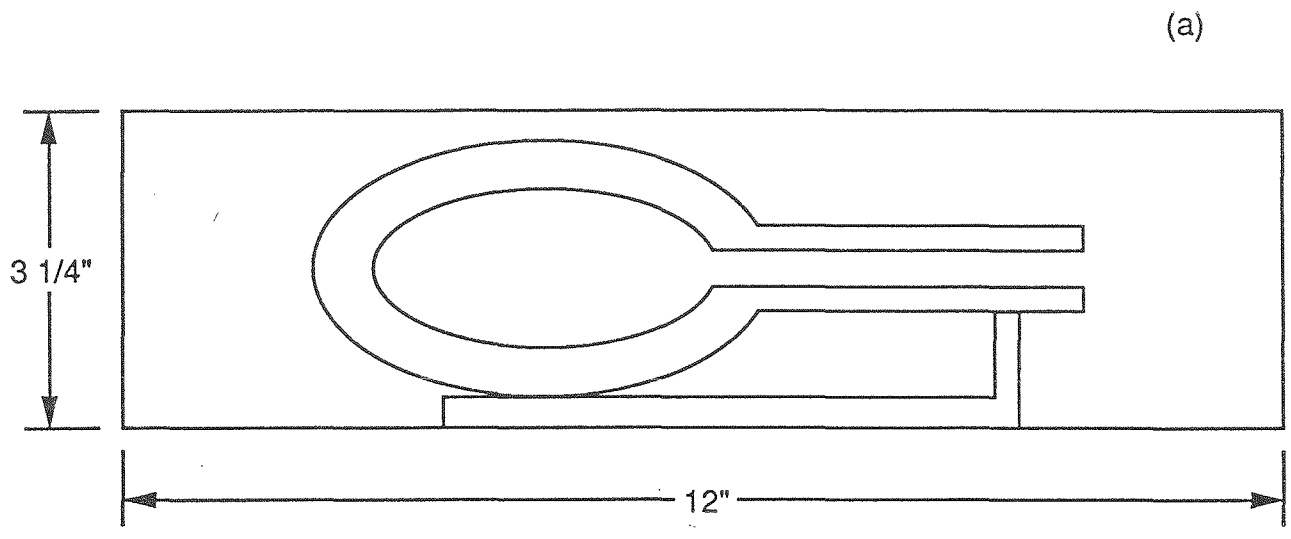


Fig. 1

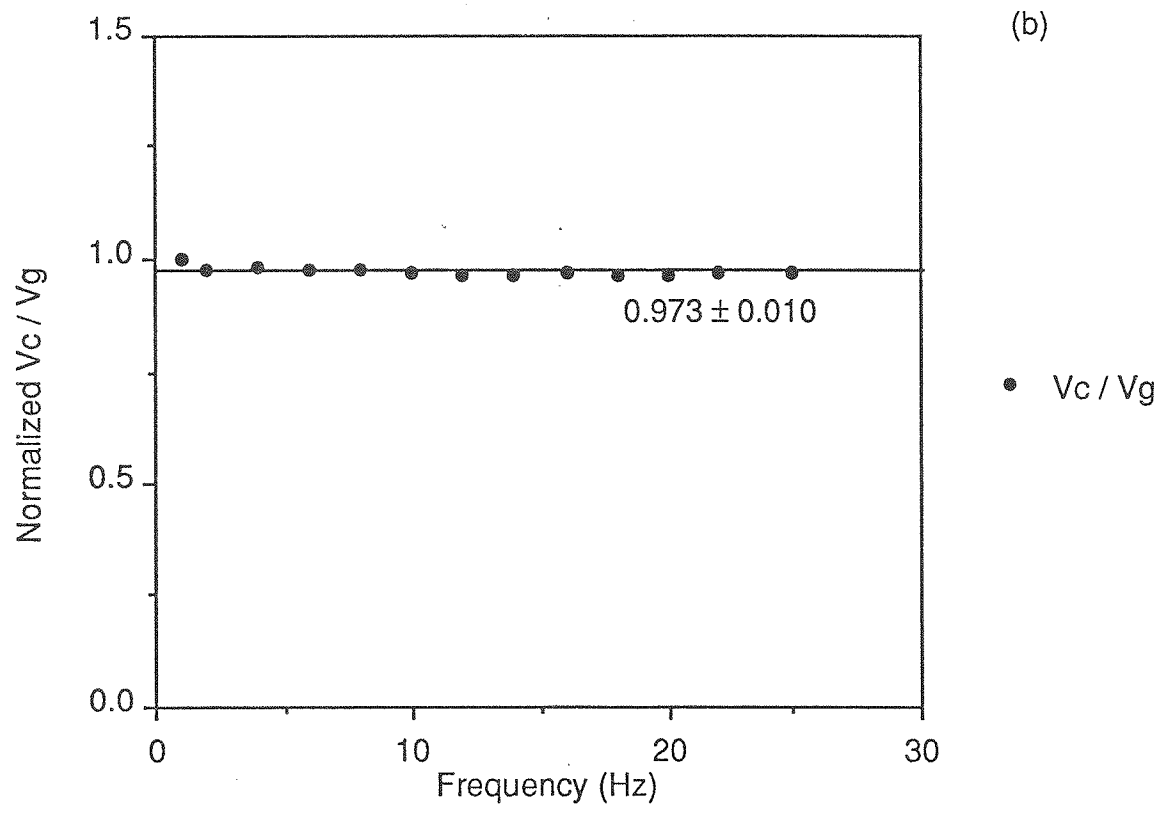
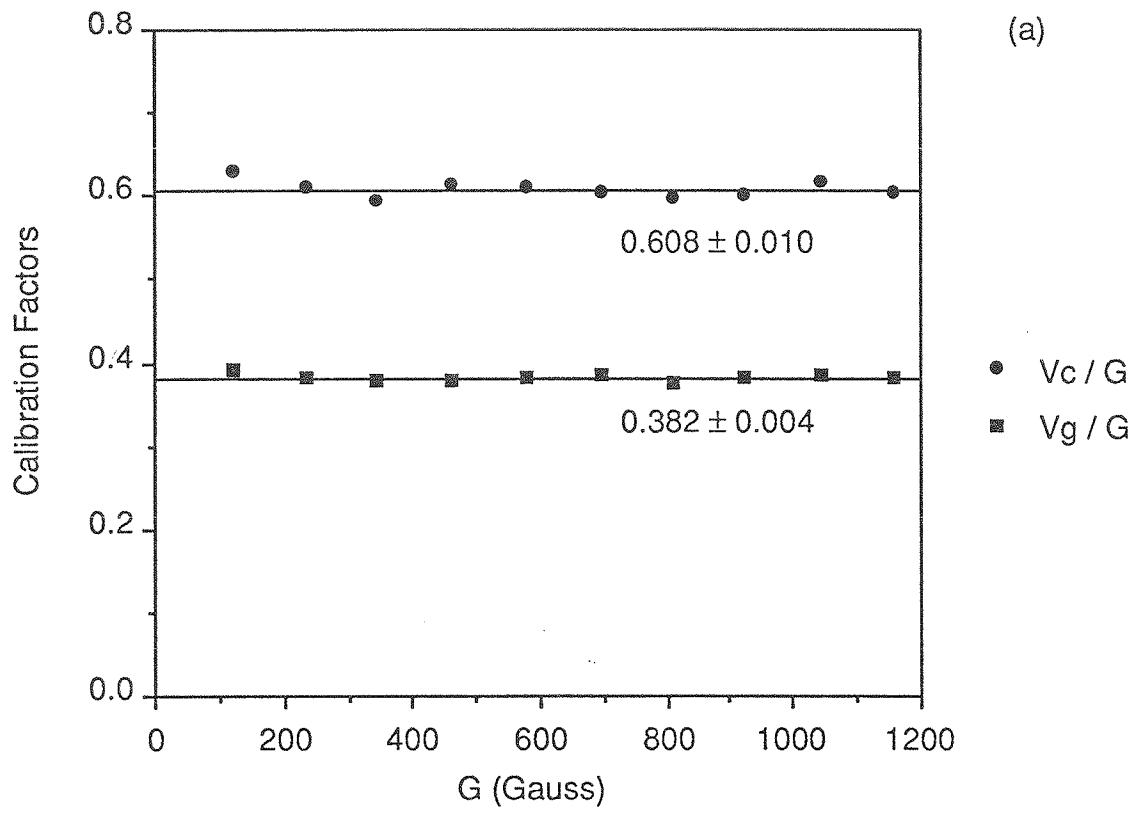


Fig. 2

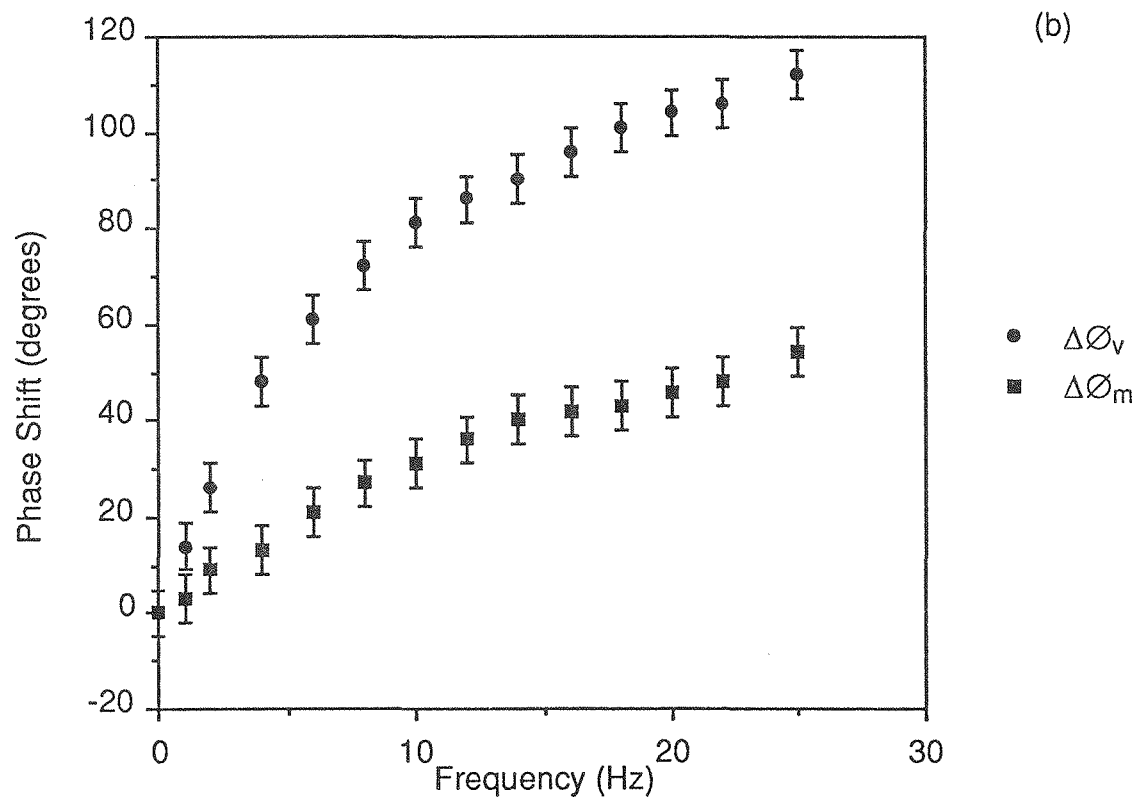
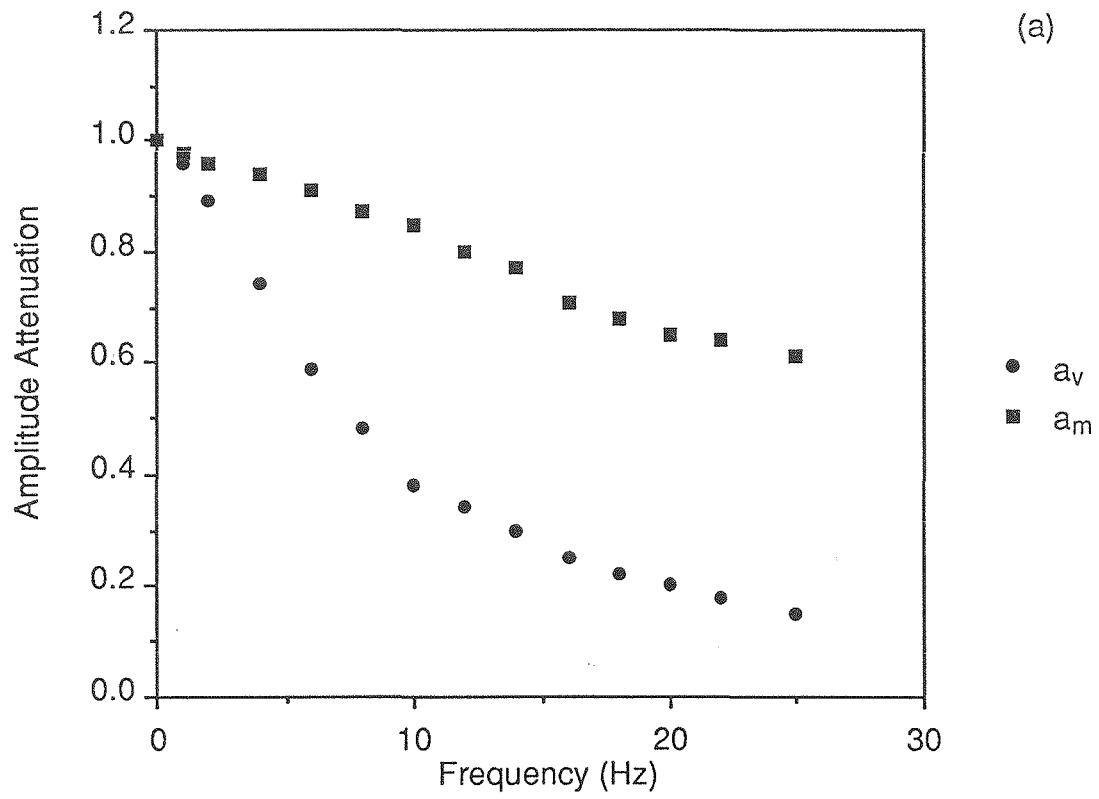


Fig. 3

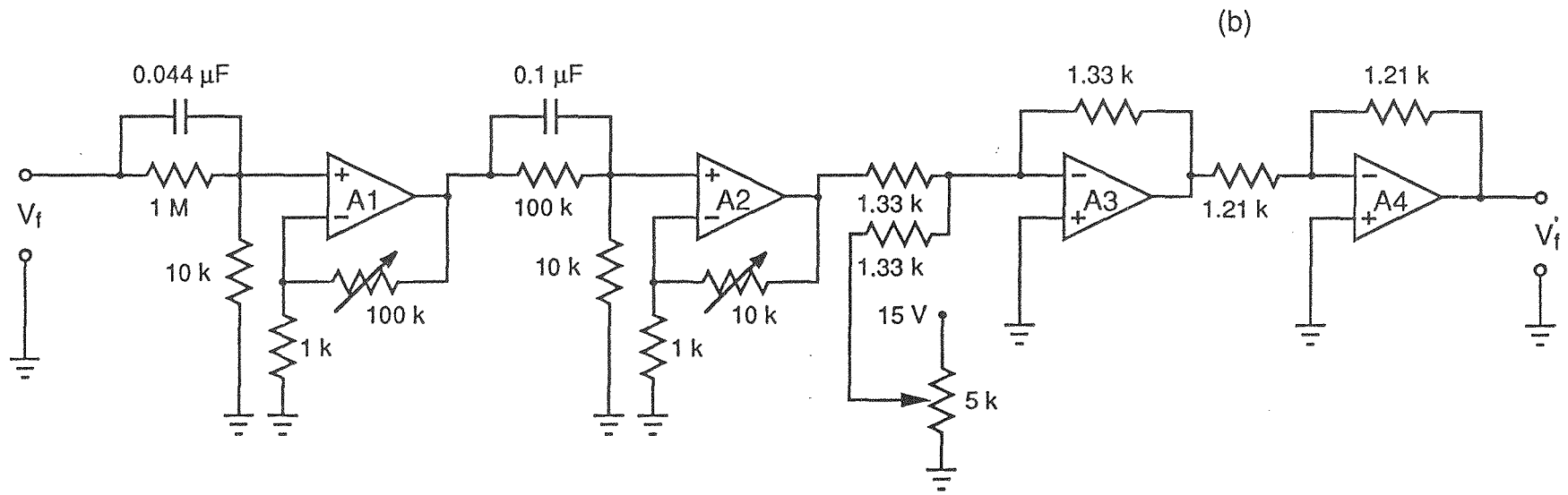
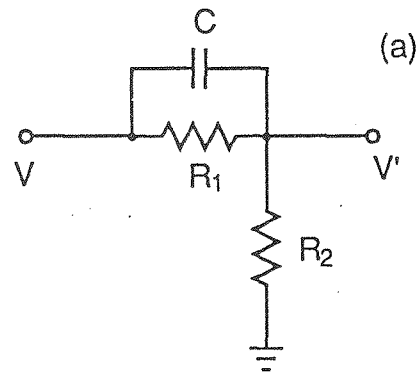


Fig. 4

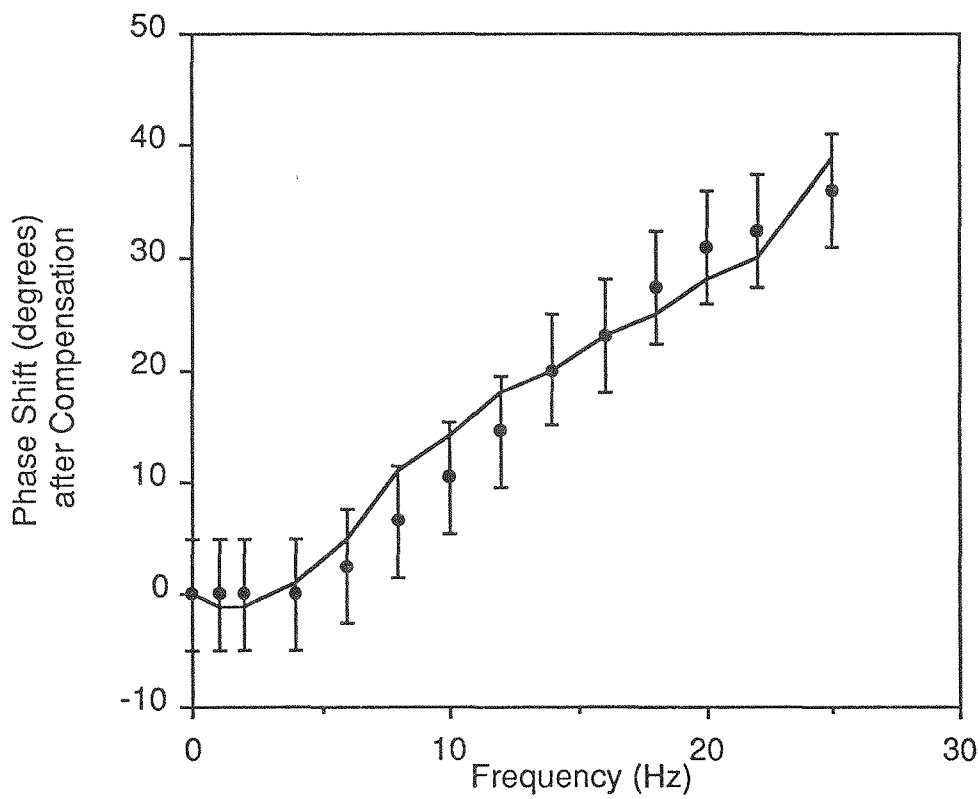
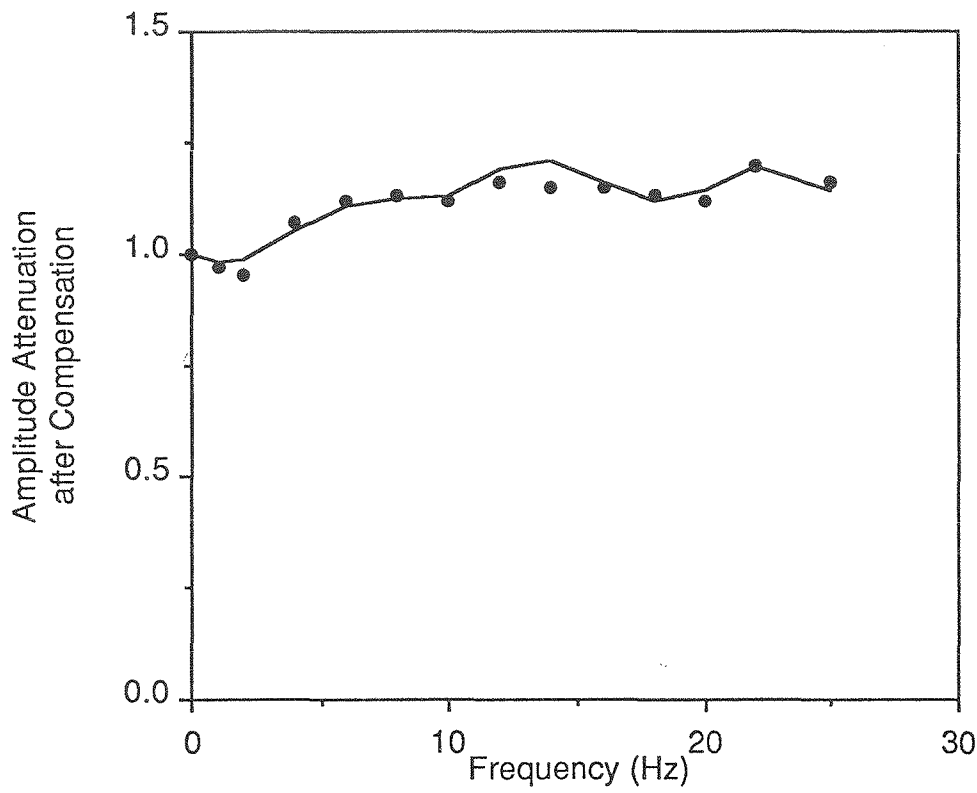
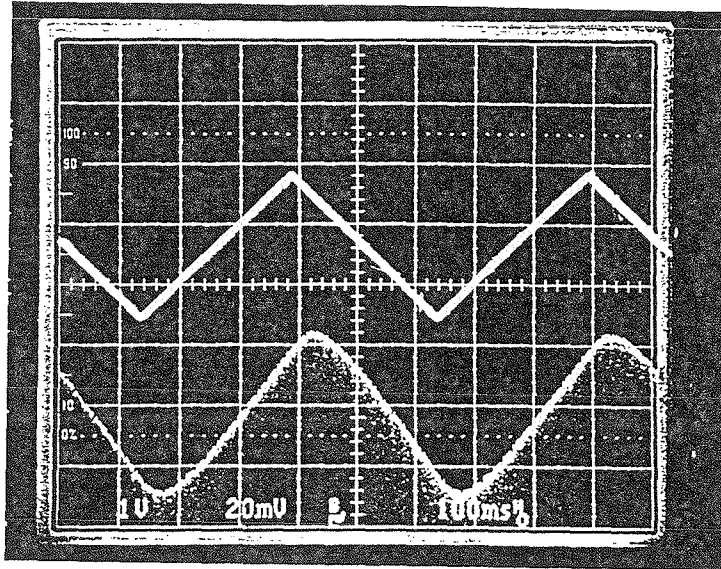
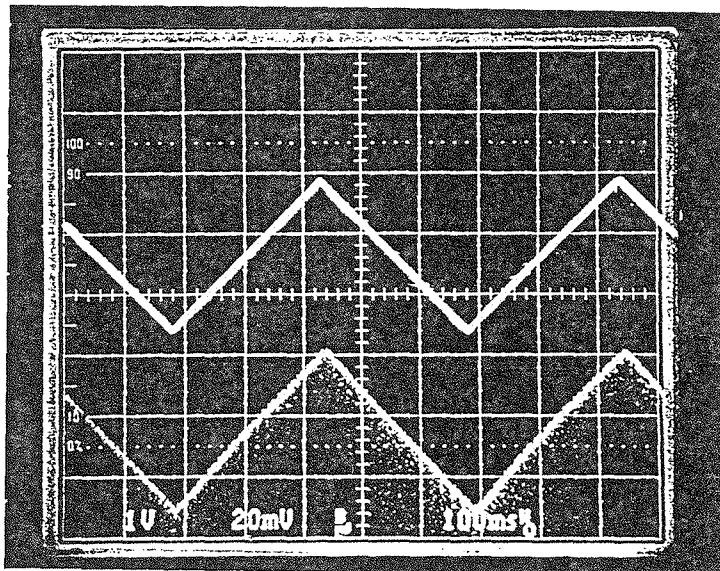


Fig. 5

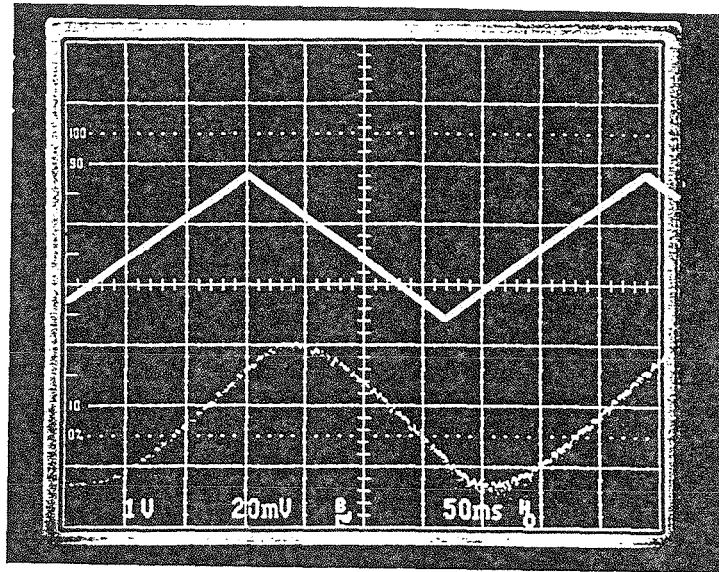


(a)

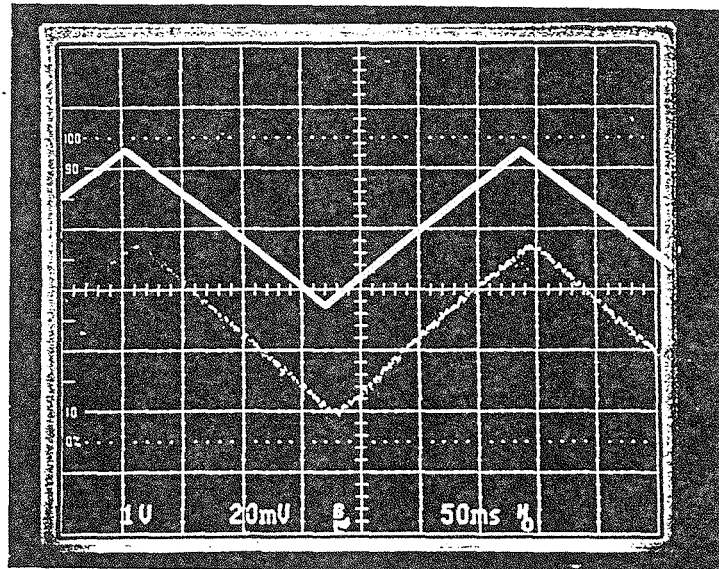


(b)

Fig. 6



(a)



(b)

Fig. 7